Elastomers and Composites
Vol. 59, No. 4, pp. 156~167 (December 2024)
Print ISSN 2092-9676/Online ISSN 2288-7725
DOI: https://doi.org/10.7473/EC.2024.59.4.156

Synthesis and Characterization of Ag/Mn-Doped TiO_2 Composites with Bacterial Inactivation under Visible Light and Its Application to Silicone Foam

Sunyoung Han[*] and Eunkyoung Lee[,†]**

[*]*Department of Pharmaceutical Biomedical Engineering, Cheongiu University, Cheongiu 28503, Republic of Korea*
[**]*Department of Applied Chemistry, Graduate School, Cheongiu University, Cheongiu 28503, Republic of Korea*

(Received December 6, 2024, Revised December 23, 2024, Accepted December 31, 2024)

Abstract: This study investigates the synthesis and characterization of Ag/Mn-TiO_2 composites, which exhibit enhanced antibacterial activity under visible light due to the doping of silver (Ag) and manganese (Mn) into titanium dioxide (TiO_2). The synthesized Ag/Mn-TiO_2 composites are analyzed using X-ray diffraction, X-ray photoelectron spectroscopy, and scanning electron microscopy to confirm their structural and chemical properties. The results reveal that metallic Ag is distributed on the surface of TiO_2, whereas Mn ions are integrated into the TiO_2 lattice. Antibacterial and antifungal activities are evaluated against *Escherichia coli* and *Aspergillus niger*, respectively, demonstrating significant inhibition (99.9% reduction) under visible light. In addition, the successful incorporation of Ag/Mn-TiO_2 composites into silicone foam results in excellent antibacterial (99.9% reduction) and antifungal (complete inhibition) effects. The findings suggest that Ag/Mn-TiO_2 composites are effective materials for enhancing microbial resistance in indoor environments, highlighting their potential for promoting cleaner and healthier indoor spaces.

Keywords: Ag/Mn-TiO_2 composites, visible light, antibacterial performances, antifungal performances, silicone foam

Introduction

With the improvement of modern living environments and advancements in science, the indoor environment has become increasingly insulated and sealed, creating an ideal condition for the growth of various germs and molds. As proliferation of these microorganisms causes damage to products and various diseases for humans, the development of sustainable antibacterial substances is essential without sanitization of the contaminated environment.[1,2] There are inorganic antibacterial agents such as silver, copper, zinc, and titanium dioxide and organic antibacterial ones such as comprise iodine compounds, alcohol, and chitosan. Inorganic antibacterial agents are preferred to organic antibacterial ones owing to their prolonged antibacterial effects and higher safety for humans.[3-9] Titanium dioxide (TiO_2) antibacterial efficiency is attributed to the oxidative damage primarily induced by reactive oxygen species (ROS), like $O_2•^-$, H_2O_2 and HO•. These reactive oxygen species are produced on the surface of TiO_2 when illuminated by UV light, exciting electrons from valence band to the conduction band thus creating electron-hole pairs. With holes (h^+) and hydroxyl radicals (OH•) generated in the valence band, and electrons and superoxide anions ($O_2•^-$) generated in the conduction band, irradiated TiO_2 photocatalysts can decompose organic compounds by oxidation reactions.[10,11] In addition, non-toxic TiO_2, has excellent photocatalytic activity and chemical stability,[12] and performs self-cleaning on material surfaces.[13] TiO_2 However, is inactive under visible light (470 nm to 750 nm) because of its wide bandgap energy which is around 3.2 eV.[10] Research has been conducted to reduce the band gap and alter the positions of the valence band and conduction band through being doped with various substances, thereby achieving photoactivation under visible light.[14-17] Incorporating metal dopants into TiO_2 functions as electron or hole site, which reduces the recombination rate of electron-holes and improves TiO_2 photocatalytic activity by narrowing the bandgap energy.[13] The antibacterial activity of Ag-TiO_2 can be attributed to two primary characteristics. Firstly, it removes contaminants through free radicals. Silver particles act as electron traps, capturing electrons transferred from the conduction band of titanium dioxide

†Corresponding author E-mail: eklee@cju.ac.kr

and transferring these electrons to oxygen, which converts them into superoxide radicals. The holes in titanium dioxide react with H_2O to form highly reactive hydroxyl radicals. These free radicals are effective in photocatalytic oxidation and bacterial inhibition.[18] Secondly, the doped silver particles have demonstrated remarkable antibacterial activity due to their microbial decomposition abilities.[19] When titanium dioxide is doped with manganese, the manganese metal ions can act as trap sites for electrons or holes, reducing the recombination rate of electrons-holes.[10] Furthermore, manganese ions can be readily incorporated into the titanium dioxide lattice due to their comparable size to titanium ions, fewer defect sites and better charge mobility.[20] Silicone foam is an eco-friendly material that exhibits properties of both silicone rubber and foam. It is used in a variety of industrial applications due to its exceptional fire stability and superior durability.[21,22]

It is employed extensively across a range of industrial sectors. In light of recent research into the enhancement of indoor materials, there is an increasing demand for the incorporation of antibacterial functionalities to improve indoor comfort. Given that the cellular structure of silicone foam facilitates microbial habitation,[23] it is imperative that the material possesses continuous antibacterial properties.

In this study, Ag/Mn-TiO_2 composite was prepared to allow antibacterial and antifungal performance in visible light by promoting electron-hole separation. Each of Ag-TiO_2 and Mn-TiO_2 was synthesized using a photodeposition and sol-gel methods, respectively, and Ag/Mn-TiO_2 composite was prepared with variation of the composition ratio and calcination between Ag-TiO_2 and Mn-TiO_2. The morphological properties of the obtained composites were investigated by scanning electron microscopy (SEM) and X-ray diffraction (XRD) analysis was used to confirm the crystallinity. The state of a chemical bond in the composites was investigated by X-ray photoelectron spectroscopy (XPS) analysis as well. The antibacterial activity of the Ag/Mn-TiO_2 against *Escherichia coli* (*E. coli*) was studied and the antifungal activity was also analyzed using *Aspergillus niger* (*A. niger*). Furthermore, an eco-friendly antibacterial silicone foam compounded with Ag/Mn-TiO_2 composites was prepared. The presence and dispersion of the Ag/Mn-TiO_2 composites were confirmed through SEM-EDS analysis and their antibacterial and antifungal activity was investigated as well.

Experimental

1. Materials

TiO_2 (Evonik Co, 80% anatase and 20% rutile), $AgNO_3$ (Daejung Co, 99.0%) and NH_4OH (Daejung Co, 25.0-30.0%) were used as precursors for the preparation of Ag-TiO_2. Tetrabutyl orthotitanate (TBOT, Daejung Co, 80%.), $MnSO_4 \cdot 5H_2O$ (Daejung Co, 98%), Acetic acid (CH_3COOH, Daejung Co, 98%) and Nitric acid (HNO_3, Daejung Co, 60%) were used to prepar Mn-TiO_2. In order to compound silicone foam with Ag/Mn-TiO_2 composite, vinyl polydimethylsiloxane(Vinyl PDMS, DMS-V41), hydroxy polydimethylsiloxane(H PDMS, DMS-H11), polyol(FLEXFOAM-iT3A) and isocyanate(FLEXFOAM-iT3B) were used without further distillation.

2. Preparation of Ag/Mn-TiO_2 composite

Deionized water with TiO_2 and $AgNO_3$ was stirred at 45°C for 2 h and the pH was adjusted using NH_4OH. Continuous magnetic stirring was performed for 30 minutes while irradiating UV to deposit the reduced Ag^+ onto the TiO_2 surface. After the prepared Ag-TiO_2 suspension was centrifuged to obtain Ag-TiO_2, it was washed with ethanol and deionized water followed by being dried, and annealed at 400°C.

For Mn-TiO_2 synthesis, ethanol dissolved with $MnSO_4 \cdot 5H_2O$ was stirred for 4 h and TBOT solution and acetic acid were sequentially added, with pH adjusted to 4 by dropwise addition of HNO_3. The mixture was stirred until gel formation, and resulting gels were dried at 100°C and annealed at 400°C.

The Ag/Mn-TiO_2 composite was synthesized by two methods; 1) a) Ag-TiO_2 and Mn-TiO_2 were dried, forming

Table 1. Composition Ratio of Ag/Mn-TiO_2 unit(g)

	Ag-TiO_2	Mn-TiO_2
1-AM19	1	9
1-AM28	2	8
1-AM37	3	7
1-AM46	4	6
2-AM19	1	9
2-AM28	2	8
2-AM37	3	7
2-AM46	4	6

gel, respectively b) the gels were mixed and c) calcinated at 400°C. 2) a) Ag-TiO_2 and Mn-TiO_2 were dried, respectively b) each of gels was calcianted at 400°C and c) mixed followed by being calcinated at 400°C again. The composition ratio between Ag-TiO_2 and Mn-TiO_2 is shown at Table 1.

A mixture of Vinyl PDMS and Ag/Mn-TiO_2 composite was prepared and blended with an isocyanate solution containing H-PDMS in order to prepare the silicone foam compounded with the Ag/Mn-TiO_2 composite, followed by being cured at 100°C for 10 min and foamed.

3. Characterization

Scanning electron microscope (SEM, JSM-7610F) was used to investigate the morphology of the prepared composite. The crystal phases of the composites were analyzed via X-ray diffractometry (XRD, JP/SmartLab) operated at 45 kV and 200 mA. X-ray photoelectron spectroscopy (XPS) was used to analyze the surface elemental composition and chemical state. XPS measurements were carried out with PHI Quantera-II (Ulvac-PHI) using Al$K\sigma$ X-ray source and C 1s (284.8 eV) was used as standard for charge correction. The dispersion and elemental composition of the Ag/Mn-TiO_2 composite within the antibacterial silicone foam were studied using an energy dispersion X-ray spectrometer (EDS, JSM-7610F).

4. Antibacterial and Antifungal studies

The antibacterial activity of the synthesized Ag/Mn-TiO_2 composites were evaluated by using *E. coli* with the 'Disk diffusion test' in accordance with NCCLS M100-S5. The suspensions of *E. coli* were sprayed over the surface of agar plates and dried at room temperature. The round disks with Ag/Mn-TiO_2 composites were placed on top of the inoculated plates and cultivated at 37°C for 24 h under visible light. The antibacterial activation was assessed by observing the width of a Zone of inhibition (ZOI) formed around disks.

To evaluate quantitative of the antimicrobial and anti-fungal activity, the percent of reduction(%) was estimated in accordance with ASTM E2149 against *Escherichia coli* (*E. coli*, ATCC 8739) and *Aspergillus niger* (*A.niger*, ATCC 6275), respectively. The Ag/Mn-TiO_2 composite was brought into contact with bacterial suspension under the sterile condition and cultivated at 25°C with strong agitation. The bacterial suspension was plated on agar plates and the colony forming units (CFU) are determined after 24 h. The antibacterial activity and antifungal efficacy were calculated by the following Eq. (1):

$$\text{Reduction Rate (\%)} = \frac{(C-T)}{C} \times 100 \quad (1)$$

where Reduction Rate(%) is the percentage of reduction bacteria viability, C is the number of viable bacteria at contact time 0 min (CFU/ml) and T is the number of viable bacteria after contact time 24 h (CFU/ml) with Ag/Mn-TiO_2 composite.

The antifungal efficacy of the silicone foam compounded with Ag/Mn-TiO_2 was evaluated in accordance with ASTM G21 standards. A suspension of *A. niger* (ATCC 6275) spores was applied to the surface of the silicone foam, which was then incubated for four weeks. The extent of fungal growth on the surface was evaluated and the results are presented in Table 2.

Table 2. Fungi Rating According to ASTM G21

Rating	Observed growth on specimens
0	None
1	Traces of growth (less than 10%)
2	Light growth (10%-30%)
3	Medium growth (30-60%)
4	Heavy growth (60% to complete coverage)

Results and Discussion

1. Synthesis of Ag/Mn-TiO_2 composites

1.1. XRD Analysis

The crystal phase and structure of the synthesized Ag/Mn-TiO_2 composites were examined by X-ray diffractometry (XRD). The XRD analysis of single TiO_2 and Ag/Mn-TiO_2 composites by Method-1 is shown in Figure 1; also shown in Figure 2. for single TiO_2 and Ag/Mn-TiO_2 composites by Method-2. All composites exhibited the anatase diffraction peak at $2\theta=25.5°$ and the rutile diffraction peak at $2\theta=27.5°$, indicating that both anatase and rutile phases are mixed. This is due to the P-25 TiO_2 used for synthesis exists in two phases: 80% anatase and 20% rutile. Furthermore, an additional peak was identified at $2\theta=32.5°$ for all composites. This is because the presence of Ag metal[24] was confirmed from the diffraction peak of Ag_2O located at $2\theta=32.5°$.

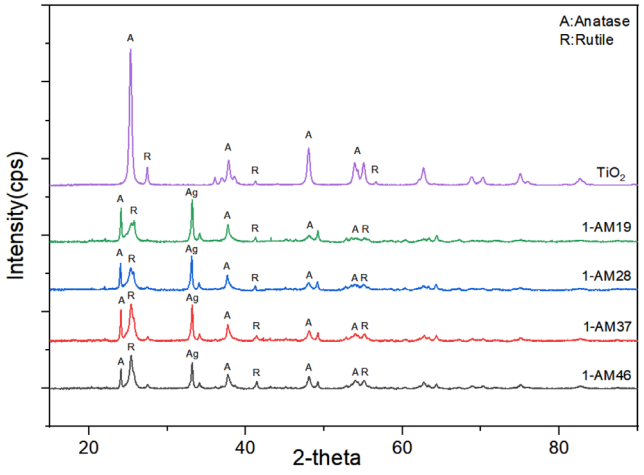

Figure 1. X-ray diffraction (XRD) patterns of TiO_2 and Ag/Mn-TiO_2 composites by Method-1.

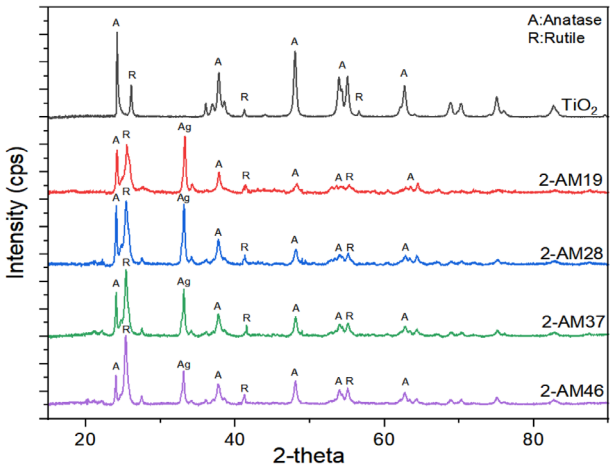

Figure 2. X-ray diffraction (XRD) patterns of TiO_2 and Ag/Mn-TiO_2 composites by Method-2.

This indicates that the Ag particles were not incorporated into the TiO_2 structure due to the large ionic radius of Ag (1.15 Å), confirming that the Ag particles were deposited in metallic form on the TiO_2 surface.[25,26] In contrast, no obvious diffraction peaks attributed to Mn (2θ=33.05°)[24] were observed, as Mn ions readily substitute for Ti^{4+} ions[27] within

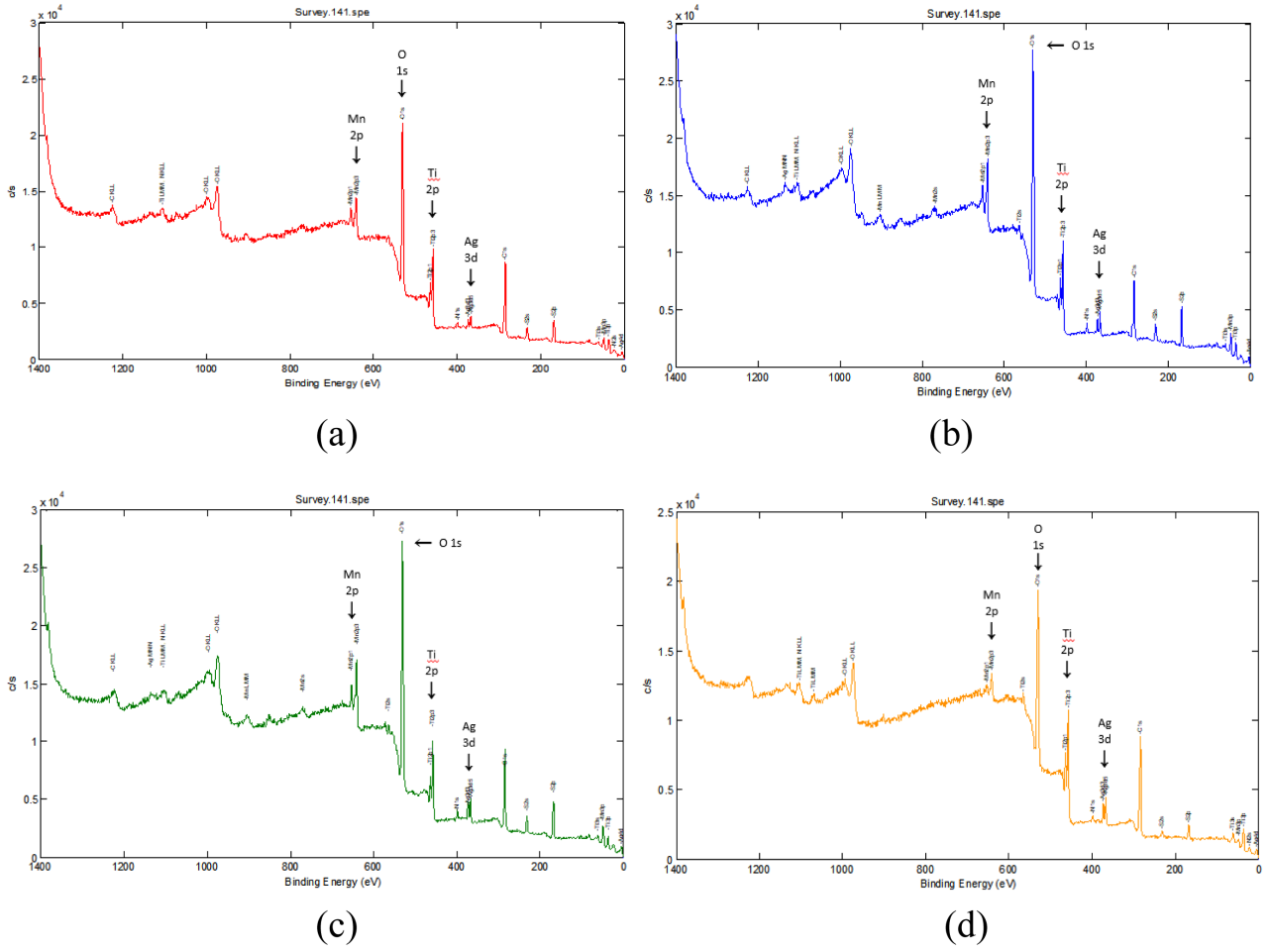

Figure 3. XPS spectra for the Ag/Mn-TiO_2 composites by Method-1; (a) 1-AM19, (b) 1-AM28, (c) 1-AM37, and (d) 1-AM46.

the lattice due to the small difference in ionic radius between Mn^{2+} (0.62 Å) and Ti^{4+} (0.68 Å)[28]. In addition, the Ag peaks of the Ag/Mn-TiO_2 composites synthesized by Method-2 are stronger than those of Ag/Mn-TiO_2 composites synthesized by Method-1 (see Figure 1 and Figure 2), which is due to the aggregation of Ag particles on the surface caused by repeated high-temperature annealing processes.[29-31] As presented in Figure 3 and Figure 4, it was confirmed that some anatase TiO_2 was converted to rutile structures with increasing Ag content. This is due to the fact that the surface defect density of Ag/Mn-TiO_2 composites increases with increasing Ag doping content, which promotes the transformation to the rutile structure. These surface defects are not only considered as rutile nucleation sites[31] but also increase the contact areas between particles, thereby facilitating the formation of the rutile structure.[32]

1.2. XPS Analysis

X-ray photoelectron spectroscopy (XPS) was utilized to characterized the elemental composition and chemical bonding state of the Ag/Mn-TiO_2 composites. Figure 3 and Figure 4 show the X-ray photoelectron spectrum of the Ag/Mn-TiO_2 composites prepared by Method-1 and Method-2, respectively. All the composites exhibit the peaks located at 458.4 eV, which were assigned to Ti 2p binding energy, corresponding to Ti^{4+} on the TiO_2 lattice. In addition, two peaks of Ag 3d binding energy were observed at 367 eV and 361.6 eV, corresponding to the characteristic binding energy of metallic silver,[33] and difference in binding energy by 6.0 eV showed that the Ag element exists in the form of metallic Ag(Ag^0).[34,35] The peak at 641.5 eV corresponds to the binding energy of Mn 2p, confirming the presence of Mn integrated into the TiO_2 lattice in the form of Mn^{2+}.[36] These results confirm the successful synthesis of Ag/Mn-TiO_2 composites in which metal Ag is dispersed on the surface and Mn is stably integrated into the TiO_2 lattice,

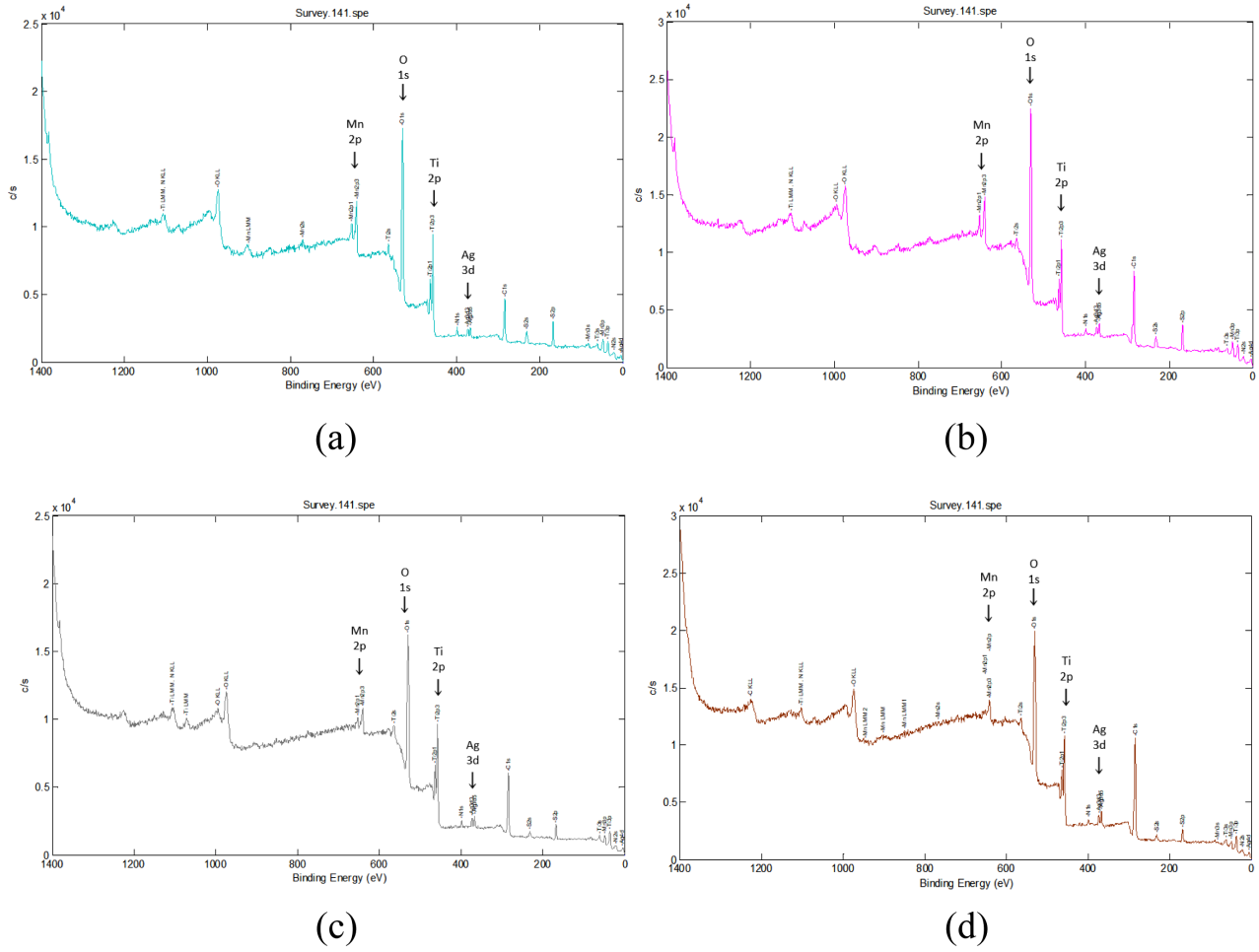

Figure 4. XPS spectra for the Ag/Mn-TiO_2 composites by Method-2; (a) 2-AM19, (b) 2-AM28, (c) 2-AM37, and (d) 2-AM46.

Table 3. XPS Surface Chemical Composition of the Ag/Mn-TiO_2 Composites unit(%)

Elemental composition (%)	Sample							
	1-AM19	1-AM28	1-AM37	1-AM46	2-AM19	2-AM28	2-AM37	2-AM46
Carbon	39.09	26.98	34.42	42.37	24.97	33.88	35.37	47.95
Nitrogen	1.70	2.19	2.00	1.80	2.43	1.91	2.33	0.88
Oxygen	44.59	50.80	47.41	42.04	52.43	47.21	45.96	39.15
Titanium	5.82	6.55	4.92	8.18	8.24	6.63	9.35	6.97
Manganese	6.97	6.24	5.77	3.48	6.34	4.91	4.43	2.97
Silver	0.36	0.62	0.62	0.75	0.41	0.42	0.44	0.47

consistent with previous XRD analysis. Table 3 presents the elemental composition of Ag/Mn-TiO_2 composites in accordance with the Ag-TiO_2 and Mn-TiO_2 composition ratio and manufacturing method. The content of Ag and Mn in the composites prepared by Method-2 is lower than that of Ag and Mn in the composites prepared by Method-1. This can be attributed to the decomposition[37,38] of these elements during the high-temperature and long annealing process, resulting in a decrease in their concentration in the Ag/Mn-TiO_2 composites.

1.3. SEM Analysis

The morphology of the synthesized Ag/Mn-TiO_2 composites was analyzed using electron scanning microscopy (SEM). As shown in Figure 5 and Figure 6, SEM images of Ag/Mn-TiO_2 prepared by Method-1 and Method-2, respectively reveal spherical shape. It was found that the Ag-TiO_2 and Mn-TiO_2 composition ratios, as well as the synthesis method, have no significant effect on particle shape, as the P-25 TiO_2 used has a spherical morphology.[39] On the other hand, as the addition ratio of Ag-TiO_2 to the Ag/Mn-TiO_2 composites increased,

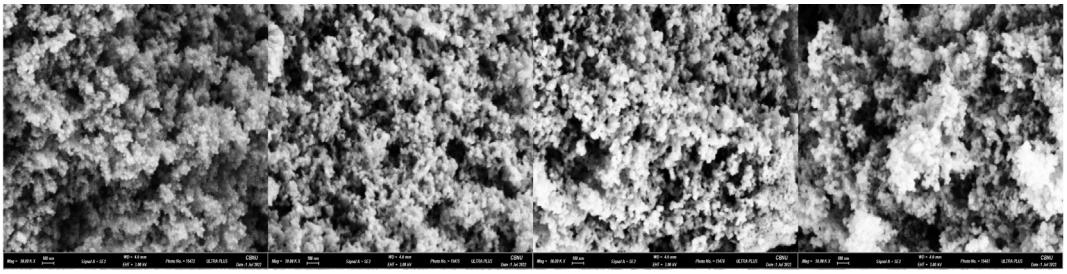

(a) (b) (c) (d)

Figure 5. SEM images of Ag/Mn-TiO_2 composites, synthesized by Method-1; (a) 1-AM19, (b) 1-AM28, (c) 1-AM37, and (d) 1-AM46.

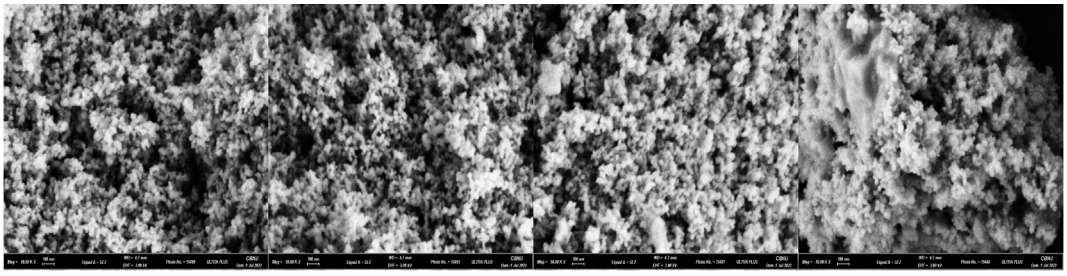

(a) (b) (c) (d)

Figure 6. SEM images of Ag/Mn-TiO_2 composites, synthesized by Method-2; (a) 2-AM19, (b) 2-AM28, (c) 2-AM37, and (d) 2-AM46.

uneven aggregates were formed. The aggregation of Ag which was not integrated into the TiO_2 structure increased on the composite surface as shown in the previous XRD and XPS analysis results. Unlike Ag, Mn was stably incorporated into the TiO_2 lattice in the form of Mn ions, and the Mn-TiO_2 particles were uniformly dispersed without agglomeration.

1.4. Antibacterial and Antifungal Performance

The antibacterial effects of Ag/Mn-TiO_2 composites were analyzed by measuring the zones of inhibition (ZOI) using disk diffusion tests against *E. coli* under visible light. The diameter of the ZOI indicates the sensitivity of the bacteria against tested samples. In accordance with the disk diffusion test results shown in Figure 7 and Figure 8, all Ag/Mn-TiO_2 composites exhibit antibacterial activity against *E. coli* compared to the pure disk, confirming their antibacterial effectiveness under visible light. The antibacterial effect of the Ag/Mn-TiO_2 composites can be attributed to the enhanced photocatalytic performance due to the synergistic

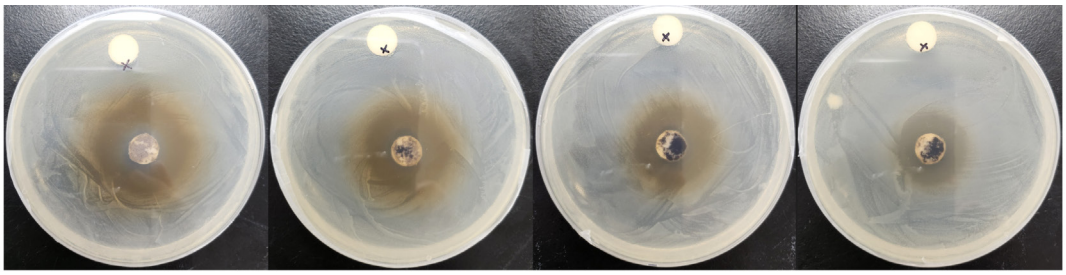

Figure 7. Antibacterial activity(disk diffusion test) of Ag/Mn-TiO_2 composites by Method-1; (a) 1-AM19, (b) 1-AM28, (c) 1-AM37, and (d) 1-AM46.

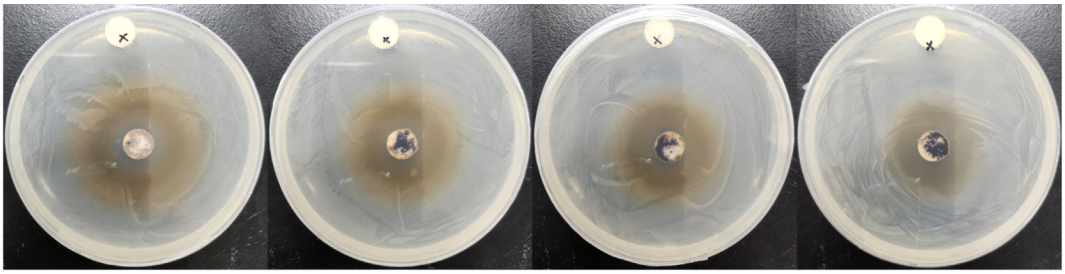

Figure 8. Antibacterial activity(disk diffusion test) of Ag/Mn-TiO_2 composites by Method-2; (a) 2-AM19, (b) 2-AM28, (c) 2-AM37, and (d) 2-AM46.

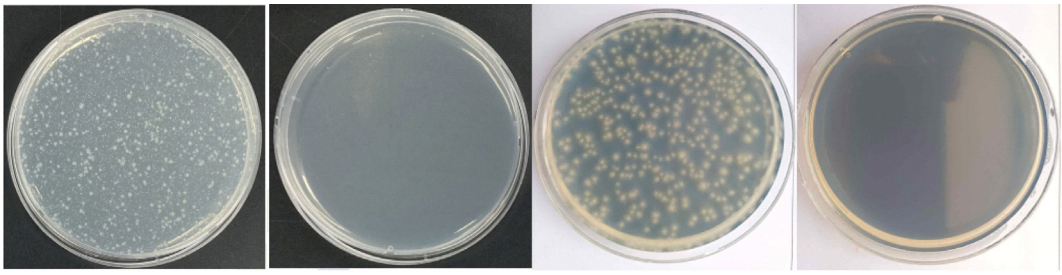

Figure 9. Antibacterial activity of 1-AM19 in accordance with ASTM E2149. (a) *E. coli* control specimen, (b) *E. coli*+1-AM19, (c) *A. niger* control specimen, and (d) *A. niger*+1-AM19.

effects of Ag and Mn dopants. The presence of Ag contributes to reactive oxygen species (ROS) production and inhibits bacterial growth through its own antibacterial properties. In addition, the incorporation of Mn extends the photocatalytic activity into the visible light spectrum by inhibiting electron-hole recombination, further enhancing ROS production and leading to more effective antibacterial performance. Moreover, as the Ag-TiO_2 content in the Ag/Mn-TiO_2 composites increased, the ZOI showed a decreasing trend. This is due to the aggregation of Ag particles dispersed on the TiO_2 surface, leading to a reduction in specific surface area and a subsequent decline in antibacterial performance. On the other hand, an increase of Mn-TiO_2 content in the Ag/Mn-TiO_2 composites enhances photocatalytic activity under visible light, which also appears to improve antibacterial performance. These results were consistent with the previous XRD and SEM analysis results. As shown in Table 3, the average ZOI for Ag/Mn-TiO_2 composites prepared by Method-1 and Method-2 was 29 mm and 27 mm, respectively, indicating that the antibacterial performance of the composites prepared by Method-1 was superior. As shown in the previous XPS analysis, the decrease for antibacterial performance can be attributed to the reduction in photocatalytic performance[31] and microbial inactivation, which occurred due to the decomposition of the Ag and Mn bonds in the composite material when prepared by Method-2. The quantitative antibacterial and antifungal activity of 1-AM19, which exhibited the most pronounced antibacterial performance, was evaluated using the shake flask method in accordance with the ASTM E2149 standard. Figure 9 shows the viable bacterial colonies on the control specimen and tested specimen after 24 h of incubation under visible light. Figure 9(a) and 9(c), representing the control specimen, show the growth of *E. coli* and *A. niger* on the LB plate, whereas no *E. coli* and *A. niger* growth is observed in Figure 9(b), (d), representing the tested specimen. The bacterial reduction rate (%) was summarized in Table 4, appearing that 1-AM19 exhibited antibacterial effects of 99.9% against both *E. coli* and *A. niger* under visible light. Thus, it was confirmed that the Ag/Mn-TiO_2 composites synthesized in this study have excellent antibacterial and antifungal properties for limiting the growth of *E. coli* and *A. niger*. These results show that the appropriate amount of doping and sintering time are important factors in improving the antibacterial and antifungal performance of Ag/Mn-TiO_2 composites.

2. Manufacture of Silicon Foam compounded with Ag/Mn-TiO_2

2.1. SEM-EDS Analysis

Scanning electron microscopy (SEM) and Energy dispersive X-ray spectroscopy (EDS) were used to analyze the surface composition of antibacterial silicone foam compounded with Ag/Mn-TiO_2. Figure 10 shows both the SEM images for a porous structure with a smooth surface and EDS elemental mapping of pure silicone foam for presence of silicon and oxygen, which correspond to the primary elements of the silicone foam. The SEM and EDS

Table 4. Inhibition Zone Diameters of Ag/Mn-TiO_2 Composites unit(mm)

Bacterial strain	Zone of inhibition (mm)							
E. coli	1-AM19	1-AM19	1-AM19	1-AM19	2-AM19	2-AM19	2-AM19	2-AM19
	31	29	28	27	30	28.5	27	25

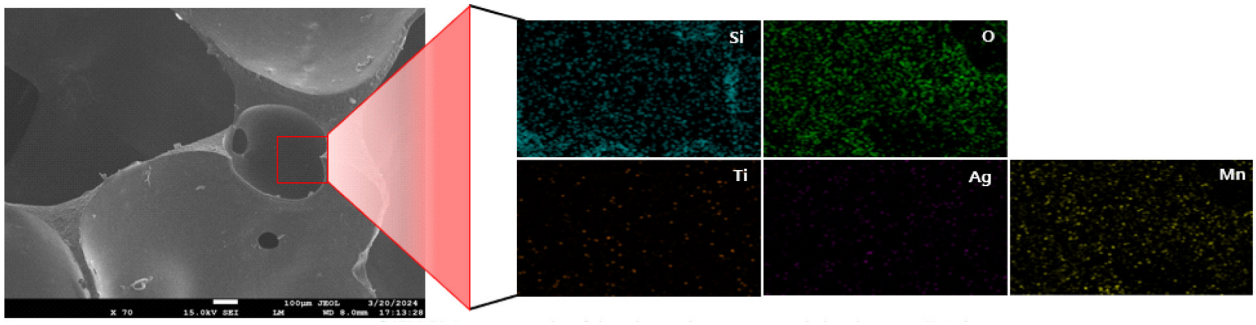

Figure 10. SEM image and EDS elemental maps of pure silicone foam.

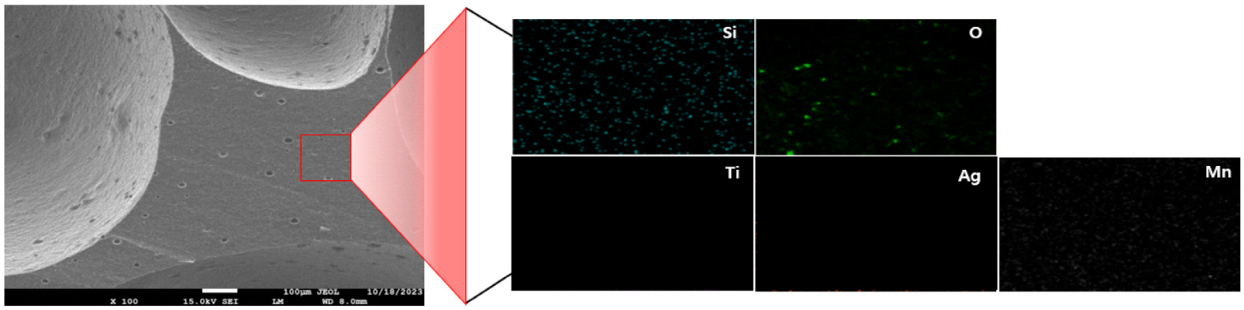

Figure 11. SEM image and EDS elemental maps of silicone foam compounded with 1-AM19.

results of the 1-AM19 compounded silicone foam are also shown in Figure 11. Silicone foam compounded with Ag/Mn-TiO_2 composite, maintained its original shape, and no morphological changes were observed due to the composite incorporation. Furthermore, the EDS elemental mapping results confirmed the presence and distribution of titanium, silver, and manganese. This suggests that the Ag/Mn-TiO_2 composite has been effectively incorporated into the silicone foam, which is expected to exhibit excellent antibacterial and antifungal properties.

2.2 Antibacterial and Antifungal Performance

The antibacterial efficacy of silicone foam compounded with Ag/Mn-TiO_2 was evaluated against *E. coli* in accordance with ASTM E2149. The antibacterial test results for the pure silicone foam and silicone foam compounded with 1-AM19 are shown in Figure 12. Pure silicone foam was completely covered by *E. coli* colonies, while growth of the *E. coli* was greatly inhibited on the silicone foam compounded with 1-AM19. Furthermore, the bacterial reduction rates are presented in Table 5, with pure silicone foam exhibiting a low bacterial reduction rate of 12.8%, whereas the silicone foam compounded with 1-AM19 demonstrated an excellent antibacterial effect, achieving a 99.9% reduction. Antifungal performance was evaluated in accordance with ASTM G21 standards and the results are shown in Figure 13. The antifungal effect was evaluated on the basis of the fungal growth after the incubation period and rated as follows: 4 for heavy growth (over 60%), 3 for medium growth (30-60%), 2 for light growth (10-30%), 1 for traces of growth (<10%), and 0 for no growth. Figure 13(a) and (b) illustrate *A. niger* growth on the surface of the 1-AM19 compounded

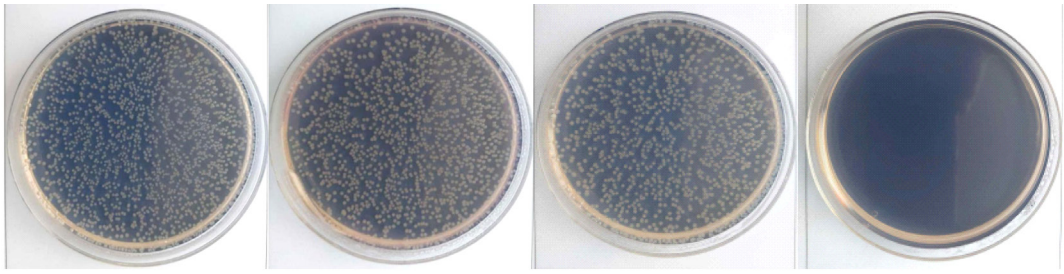

Figure 12. Antibacterial activity of pure silicone foam and silicone foam compound with 1-AM19. (a) *E. coli* control specimen, (b) *E. coli*+pure silicone foam, (c) *E. coli* control specimen, and (d) *E. coli*+silicone foam compounded with 1-AM19.

Table 5. The Bacterial Reduction rate(%) for 1-AM19 in Accordance with ASTM E2149

Test strain	Inoculated concentration (CFU/mL)	Residual amount of bacteria (CFU/mL)		Reduction rate (%)
		Control specimen	Tested specimen	
E. coli (ATCC 8739)	2.7×10^5	2.1×10^5	< 10	99.99
A. niger (ATCC 6275)	2.9×10^5	2.3×10^5	< 10	99.9

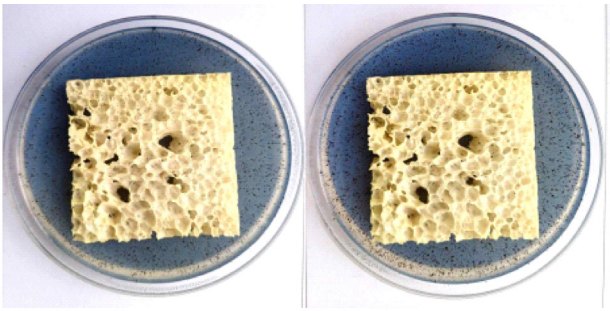

(a) (b)

Figure 13. Surface fungal growth of silicone foam compounded with 1-AM19 against *A. niger* (a) 2 weeks and (b) 4 weeks.

Table 6. Results of the Percentage Reduction of *E. coli* of Pure Silicone Foam and Silicone Foam Compounded with 1-AM19

	Pure silicone foam	Silicone foam compounded with 1-AM19
B_0	2.3×10^5	2.3×10^5
B_{24}	7.8×10^6	7.8×10^6
A_{24}	6.8×10^6	< 10
Reduction Rate (%)	12.8	99.9

*B_0: Initial number of bacteria in the control sample A_{24}: Number of bacteria in the test sample after 24 h of incubation B_{24}: Number of bacteria in the control sample after 24 h of incubation

Table 7. Specimen Surface Fungal Growth Rate after an Incubation Period of 4 weeks

		Silicone foam compounded with 1-AM19
Rating	1 weeks	0
	2 weeks	0
	3 weeks	0
	4 weeks	0

silicone foam after 2 weeks and 4 weeks, respectively with no fungal growth observed. The results of fungal growth for 4 weeks are presented in Table 6, with a growth rating of 0, confirming its excellent antifungal properties. As shown in the previous SEM-EDS analysis, this suggests that the Ag/Mn-TiO_2 composite was effectively compounded into the silicone foam, contributing to its high antibacterial and antifungal performance due to the superior photocatalytic effect of Mn and the bacterial inactivation effect of Ag. Therefore, it can be concluded that the 1-AM19-compounded silicone foam synthesized in this study exhibits excellent antibacterial and antifungal performance against both *E. coli* and *A. niger* under visible light.

Conclusions

In this study, Ag/Mn-TiO_2 composites with improved antibacterial and antifungal activity under visible light by doping silver and manganese into the TiO_2 were successfully synthesized and characterized. The photodeposition method was used for the synthesis of Ag-TiO_2, and sol-gel method was applied for the manufacture of Mn-TiO_2. Ag/Mn-TiO_2 was synthesized by varying the composition ratio of Ag-TiO_2 and Mn-TiO_2 and calcination conditions. The structural and elemental analyses confirmed that the synthesized composite was spherical and coexisted in anatase and rutile phases. Furthermore, Ag was dispersed only on the TiO_2 surface, while Mn was stably integrated into the lattice, both contributing to enhanced antimicrobial properties. In addition, repetitive annealing resulted into the aggregation of Ag on the surface for the Ag/Mn-TiO_2 composites prepared by method-2. As the amount of Ag-TiO_2 increased, the structure transitioned from anatase to rutile phase. The 1-AM19 composite exhibited the largest zone of inhibition (ZOI) and demonstrated excellent antibacterial and antifungal performance, with a 99.9% effectiveness against *E. coli* and *A. niger*. When Ag/Mn-TiO_2 compounded into silicone foam, maintained its structural integrity and significantly improved the foam's antimicrobial efficacy. These results suggest the potential of the Ag/Mn-TiO_2 composites as effective antibacterial and antifungal materials for various applications, such as in foams.

Acknowledgement

This work was supported by the Technology Innovation Program (20010265) funded By the Ministry of Trade, Industry & Energy (MOTIE, Republic of Korea).

Conflict of Interest: The authors declare that there is no conflict of interest.

References

1. B. Gaur, B. Lochab, V. Choudhary, and I. K. Varma, "Azido Polymers-Energetic Binders for Solid Rocket Propellants" *Macromolecular Science*, **43**, 505 (2003).
2. K. H. Hong and T. J. Kang, "The Photocatalytic Degradation Properties of PET and Nylon 6 Fabrics Treated with Nano

TiO_2", *Textile Science and Ehgineering*, **42**, 235 (2005).
3. M. Chen, Z. Yang, H. Wu, X. Pan, X. Xie, and C. Wu, "Antimicrobial activity and the mechanism of silver nanoparticle thermosensitive gel", *Int. J. Nanomedicine*, **15**, 2873 (2011).
4. W. C. Oh, J. G. Kim, and M. K. Kim, "A Study on the Surface and Antibacterial Properties for M(Cd, Cu)-Activated Carbon", *The Korean Society of Analytical Sciences*, **12**, 105 (1999).
5. K. R. Raghupathi, R. T. Koodali, and A. C. Manna, "Size-Dependent Bacterial Growth Inhibition and Mechanism of Antibacterial Activity of Zinc Oxide Nanoparticles", *Langmuir*, **27**, 4020 (2011).
6. S. H. Roh, J. K. Kim, and Y. S. Cho, "Synthesis of Macroporous TiO_2 Microparticles for Anti-Bactericidal Application", *Korean Chemical Engineering Research*, **56**, 524-535 (2018).
7. S. Y. Kim, K. P. Noh, H. K. Kim, S. G. Kim, J. K. Kook, S. N. Park, M. J. Kim, J. J. Kim, and E. S. Kim, "Saliary bacterial counts after application of povidone-iodine and chlorhexidine", *Korean Assoc Oral Maxillofac Surg*, **35**, 312 (2009).
8. E. K. Lee and Y. K. Kim, "A Study on the Synthesis and Antimicrobial Properties of the Chitosan Derivatives", *Elastomers and Composites*, **56**, 254 (2021).
9. Y. J. Ji and J. S. Jeong, "Comparison of Antimicrobial Effect of Alcohol Gel according to the Amount and Drying Time in Health Personnel Hand Hygiene", *J. Korean Acad Nurs.*, **43**, 305 (2013).
10. M. C. Kim, "The characteristics of Mn-TiO_2 catalyst for visible-light photocatalyst", *Analytical Science & Technology*, **24**, 493 (2011).
11. A. J. Haider, R. H. AL-Anbari, G. R. Kadhim, and C. T. Salamc, "Exploring potential Environmental applications of TiO_2 Nanoparticles", *Energy Procedia*, **119**, 332 (2017).
12. A. A. Ashkarrana, H. Hamidinezhad, H. Haddadi, and M. Mahmoudi, "Double-doped TiO_2 nanoparticles as an efficient visible-light-active photocatalyst and antibacterial agent under solar simulated light", *Applied surface science*, **301**, 338 (2014).
13. M. Ahmadi, S. M. Alavi, and A. Larimi, "Effective CO_2 photoreduction to methane over Bi_2MoO_6/Ni, N co-doped TiO_2 nano-photocatalyst", *International Journal of Hydrogen Energy*, **56**, 1309 (2024).
14. J. Moon, C. Y. Yun, K. W. Chung, M. S. Kang, and J. Yi, "Photocatalytic activation of TiO_2 under visible light using Acid Red 44", *Catalysis Today*, **87**, 77 (2003).
15. Z. Elafia, M. Y. Messous, B. Hammouti, and M. Cherkaoui, "Synthesis and characterization of Mn/Ce-Doped TiO_2: Investigation of structural and optical properties", *Moroccan Journal of Chemistry*, **11**, 350 (2023).
16. S. Cho, Y. I. Lee, L. H. Kim, and D. W. Jung, "Photocatalytic and Antipathogenic Effects of TiO_2/Cu_xO ($1<x<2$)", *Korean Chemical Society*, **57**, 4 (2013).
17. E. K. Lee and S. Y. Han, "Synthesls and Characterization of the Ag-TiO_2" *Elastomers and Composites*, **57**, 1 (2022).
18. R. Khalid, and Z. Hussain, "Minireview: Silver-Doped Titanium Dioxide and Silver-Doped Zinc Oxide Photo-catalysts", *Nanotechnology*, **5**, 892 (2017).
19. M. R. Khan, T. W. Chuan, A. Yousuf, M. N. K. Chowdhury, and C. K. Cheng, "Schottky barrier and surface plasmonic resonance phenomena towards the photocatalytic reaction: study of their mechanisms to enhance photocatalytic activity", *Catalysis Science & Technology*, **5**, 2522 (2015).
20. D. P. Ojha, M. B. Poudel, and H. J. Kim, "Investigation of electrochemical performance of a high surface area mesoporous Mn doped TiO_2 nanoparticle for a super-capacitor", *Materials Letters*, **264**, 127363 (2020).
21. S. Lee and S. J. Moon, "Preparation and characterization of poly(dimethylsiloxane) foamprepared by hydrogen condensation reaction", *The Korean Society of Applied Science and Technology*, **33**, 802 (2016).
22. Y. H. Kim, H. W. Joeng, K. W. Lee, S. S. Hwang, and S. E. Shim, "Mechanical and Thermal Properties of Environmentally Benign Silicone Foam Filled with Wollastonite", *Elastomers and Composites*, **55**, 300 (2020).
23. C. H. Hong, S. H. Kim, and T. W. Hwang, "Development of Antimicrobial Polyurethane Foam for Automotive Seat Modified by Urushiol", *Korea Polymer*, **30**, 402 (2006).
24. S. P. Prakoso, A. Taufik, and R. Saleh, "One-step microwave-assisted colloidal synthesis of hybrid silver oxide/silver nanoparticles: characterization and catalytic study", *IOP Conference Series Materials Science and Engineering*, **188**, 135 (2017).
25. X. H. Gao, B. H. Zhou, and R. F. Yuan, "Doping a metal (Ag, Al, Mn, Ni and Zn) on TiO_2 nanotubes and its effect on Rhodamine B photocatalytic oxidation", *Environmental Engineering Research*, **20**, 329 (2015).
26. D. Cruz, H. B. Ortiz-Oliveros, R. M. Flores-Espinosa, P. A. Perez, I. I. Ruiz-Lopez. and K. F. Quiroz-Estrada, "Synthesis of Ag/TiO_2 composites by combustion modified and subsequent use in the photocatalytic degradation of dyes", *Journal of King Saud University*, **34**, 101966 (2022).
27. A. D. Zhu, H. G. Xu, Y. Yin, H. Liu, J. Wang, Y. Pu, W. Feng, and S. H. Chen, "Effects of Ag^0-modification and Fe^{3+}-doping on the structural, oprical and photocatalytic properties of TiO_2" *The Royal Society of Chemistry*, **9**, 4003 (2019).

28. N. Jayasaranya, R. E. Pavai, S. Sagadevan, L. Balu, and C. Manoharan, "Unveiling of Mn doped TiO_2 nanoparticles for efficient room temperature gas sensing performance", *Inorganic Chemistry Communications*, **162**, 112168 (2024).
29. S. M. Kim, J. M. Oh, and S. M. Koo, "Annealing Effect on controlling Self-Organized Ag/Ti Nanoparticles on 4H-SiC Substrat", *Ikeee*, **20**, 177 (2016).
30. J. H. Son, Y. H. Song, and J. L. Lee, "Structural Analysis of Ag Agglomeration in Ag-based Ohmic Contact to p-type GaN", *The Korean Vacuum Society,* **20**, 127 (2011).
31. B. Xin, L. Jing, Z. Ren, B.Wang, and H. Fu, "Effects of Simultaneously Doped and Deposited Ag on the Photocatalytic Activity and Surface States of TiO_2", *Physical Chemistry*, **109**, 2805 (2005).
32. S. H. Park, "The effects of reinforcing particles on the sintering properties od powder processed Al-Cu base composite", *Ajou University* (2007).
33. J. H. Lee, J. I. Youn, Y. J. Kim, and H. J. Oh, "Effects of Surface Characteristics of TiO_2 Nanotublar Composite on Photocatalytic Activity", *Materials Research*, **24**, 556 (2014).
34. J. Kim, N. Hasan, K. D. Tran, H. T. M. Truong, and S. Kim, "Degradation of organic compounds in the dark using pre-illuminated Ag/TiO_2 as a reusable Fenton-like material", *Environmental Technology & Innovation*, **32**, 103323 (2023).
35. H. Shi, Y. Yu, Y. Zhang, X. Feng, X. Zhao, H. Tan, S. U. Khan, Y. Li, and E. Wang, "Polyoxometalate/TiO_2/Ag composite nanofibers with enhanced photocatalytic performance under visible light", *Applied Catalysis B: Environmental,* **221**, 280 (2018).
36. S. Li, Z. Mu, H. Chen, Y. Yang, T. Xie, and Y. Lin, "Visible light-assisted efficient degradation of Rhodamine B by N-TiO_2/Mn-HPMo/Ag ternary composites", *Materials Research Bulletin*, **167**, 112436 (2023).
37. S. B. Hong, O. Y. Kang, S. Y. Hwang, Y. M. Heo, J. W. Kim, and B. G. Choi, "Synthesis of MnO_2 Nanowires by Hydrothermal Method and their Electrochemical Characteristics", *Applied Chemistry for Engineering*, **27**, 653 (2016).
38. K. H. Cho, J. H. Park, and C. H. Shin, "Low Temperature CO Oxidation over Cu-Mn Mixed Oxides", *The Korean Society of Clean Technology*, **16**, 132 (2010).
39. A. M. Abdullah, N. J. Al-Thani, K. Tawbi, and H. Al-Kandari, "Carbon/nitrogen-doped TiO_2: New synthesis route, characterization and application for phenol degradation", *Arabian Journal of Chemistry*, **9**, 229 (2016).